AGU ADVANCING EARTH AND SPACE SCIENCE

Geophysical Research Letters®

RESEARCH LETTER
10.1029/2022GL099048

Southern Control of Interhemispheric Synergy on Glacial Marine Carbon Sequestration

Jinlong Du[1], Ying Ye[2], Xu Zhang[3], Christoph Völker[2], and Jun Tian[1]

[1]State Key Laboratory of Marine Geology, Tongji University, Shanghai, China, [2]Alfred Wegener Institute, Helmholtz Centre for Polar and Marine Research, Bremerhaven, Germany, [3]Group of Alpine Paleoecology and Human Adaptation (ALPHA), State Key Laboratory of Tibetan Plateau Earth System, Resources and Environment (TPESRE), Institute of Tibetan Plateau Research, Chinese Academy of Sciences, Beijing, China

Key Points:

- The stepwise glacial atmospheric pCO_2 decrease is linked to a Southern Ocean (SO)-controlled synergy of interhemispheric mechanisms
- Sea ice prevents CO_2 outgassing increasingly from the early- to later-glacial time
- The SO contribution to the global biological carbon pump might increase from interglacial to glacial periods

Supporting Information:

Supporting Information may be found in the online version of this article.

Correspondence to:

J. Tian and X. Zhang,
tianjun@tongji.edu.cn;
xu.zhang@itpcas.ac.cn

Citation:

Du, J., Ye, Y., Zhang, X., Völker, C., & Tian, J. (2022). Southern control of interhemispheric synergy on glacial marine carbon sequestration. *Geophysical Research Letters*, *49*, e2022GL099048. https://doi.org/10.1029/2022GL099048

Received 6 APR 2022
Accepted 4 AUG 2022

Author Contributions:

Conceptualization: Jinlong Du, Ying Ye, Xu Zhang, Christoph Völker, Jun Tian
Data curation: Jinlong Du
Formal analysis: Jinlong Du
Funding acquisition: Ying Ye, Xu Zhang, Christoph Völker, Jun Tian
Investigation: Jinlong Du
Methodology: Ying Ye, Christoph Völker
Project Administration: Xu Zhang, Christoph Völker, Jun Tian
Resources: Xu Zhang
Software: Ying Ye, Christoph Völker
Supervision: Jun Tian
Visualization: Jinlong Du
Writing – original draft: Jinlong Du, Ying Ye, Xu Zhang, Christoph Völker, Jun Tian
Writing – review & editing: Jinlong Du, Ying Ye, Xu Zhang, Christoph Völker, Jun Tian

Abstract Among mechanisms accounting for atmospheric pCO_2 drawdown during glacial periods, processes operating in the North Atlantic (NA) and Southern Ocean (SO) have been proposed to be critical. Their individual and synergic effects during a course of glaciation, however, remain enigmatic. We conducted simulations to examine these effects at idealized glacial stages. Under early-glacial-like conditions, cooling in the SO can trigger an initial pCO_2 drawdown while the associated sea ice expansion has little impact on air-sea gas exchange. Under later glacial-like conditions, further cooling in the NA enhances ocean carbon uptake due to a stronger solubility pump, and the SO-induced stronger deep stratification prevents carbon exchange between the deep and upper ocean. Meanwhile, strengthened dust deposition increases the SO contribution to the global biological pump, and CO_2 outgassing is suppressed by fully extended sea ice cover. More carbon is then stored in the deep Pacific, acting as a passive reservoir.

Plain Language Summary CO_2 is one of the most important "greenhouse" gases that drive global climate changes. Tens of thousands of years ago, during the glacial time (known as the "ice age"), atmospheric CO_2 was much lower than today. Research has shown that processes in different ocean regions, such as the Southern Ocean (SO) and North Atlantic (NA), made essential contributions to the glacial CO_2 drawdown. However, the interplay between these processes remains unclear. Here, using an ocean general circulation model coupled with an atmospheric box that includes active air-sea CO_2 exchange, we examined the key processes at idealized stages of a glacial cycle. We found that: at an early stage, surface cooling in the SO triggers the CO_2 decrease by shortening the time for air-sea CO_2 exchange; during a late stage, the SO and NA cooling act collaboratively to store more carbon in the deep ocean, where the SO plays a more determining role. Pacific seems to be a passive carbon pool during glaciation. Sea ice expansion hinders CO_2 outgassing increasingly over the course of glaciation. Further CO_2 decrease is achieved by a larger contribution of the SO to the global biological carbon pump.

1. Introduction

What caused the atmospheric pCO_2 (pCO_2^{atm}) drawdown by ~90 ppm during glacial times (Lüthi et al., 2008) is one of the most contentious questions in earth science. The ocean has been acknowledged as the primary sink of the atmospheric carbon, as it is the largest active carbon reservoir operating at the glacial-interglacial (G-IG) timescales (Hülse et al., 2017; Sigman et al., 2020). Ocean processes, both physical and biogeochemical, are therefore intricately involved in air-sea carbon partitioning.

Distribution of freshwater, heat, and geochemical tracers throughout the interior of the global ocean is determined mainly by the two meridional overturning circulation (MOC) cells (Marshall & Speer, 2012; Talley, 2013). Both cells originate in the polar region, with Antarctic Bottom Water (AABW) formation in the high-latitude Southern Ocean (SO) and North Atlantic Deep Water (NADW) formation in the subpolar North Atlantic (NA). During glacial times, cooling of the polar regions leads to large-scale reorganization of the upper and deep cells of the MOC, featuring a shoaling of the Atlantic meridional overturning circulation (AMOC; Curry & Oppo, 2005; Lippold et al., 2012), associated with a more stratified deep ocean (Adkins, 2002).

Several processes in the high-latitude SO have been suggested to be central in explaining pCO_2^{atm} drawdown during G-IG cycles. First, a more stratified deep ocean might hold more carbon by reducing the exchange between the deep and surface ocean (Ferrari et al., 2014; Hain et al., 2010; Sigman & Boyle, 2000). Second, expansion of

sea ice-covered area in the SO could prevent ocean outgassing and enhance oceanic carbon storage (Marzocchi & Jansen, 2019; Stein et al., 2020; Stephens & Keeling, 2000). Third, higher iron supply in the SO during peak glacial times would drive pCO_2^{atm} down by stimulating biological productivity (Yamamoto et al., 2019), that is, the Iron Hypothesis (Martin, 1990). On the other hand, due to the drastic cooling of the high-latitude NA during the Last Glacial Maximum (LGM; ~21 ka), the enhanced solubility pump may make the surface carbon uptake in the NA two times more efficient compared to the Holocene state (Yu et al., 2019). A modeling study further shows that the impact per unit area of SST change on pCO_2^{atm} is much larger in the high-latitude NA than in other regions (Kurahashi-Nakamura et al., 2010). The deep North Pacific (NP) is a significant oceanic carbon reservoir and recent multiproxy reconstructions demonstrate a Pacific-wide increase in respired carbon storage during the last ice age, which is attributed to changes in physics and biological productivity originating in the SO rather than in the Pacific itself (Jacobel et al., 2019; Rae & Broecker, 2018). Nevertheless, the relationship of changes in physics and biological productivity in different ocean regions and their working together on glacial pCO_2 drawdown remains elusive.

The glacial pCO_2^{atm} drawdown can be divided into different stages (Kohfeld & Chase, 2017, Figure S1a in Supporting Information S1). During the last glacial cycle, pCO_2^{atm} decreased roughly by ~35, ~40, and ~10 ppm between Marine Isotope Stages (MIS) 5e to 5d, MIS 5a to 4, and MIS 3 to 2, respectively. These steps of pCO_2^{atm} decrease may reflect different CO_2-lowering processes acting in a sequential manner during glaciation. For example, the SO sea ice appears to have expanded at the glacial inception (Wolff et al., 2006), while the final establishment of deep stratification may have occurred at MIS 4 (Oliver et al., 2010). Iron fertilization occurred only in the coldest stages of the glacial cycle, especially at LGM (e.g., Martinez-Garcia et al., 2014). Since these processes happen at different stages of a glacial cycle, a specific process would either have impacts across the full course of glacial cycles or just over a specific time interval. In this study, we conduct idealized snapshot simulations to investigate the impacts of operating processes on glacial pCO_2^{atm} drawdown. Since temporal changes in SST and sea ice are spatially distinct in the course of glaciation, we use simulations with stepwise changes in these forcing factors as a surrogate to investigate the role of surface cooling and sea ice expansion at different stages of a glacial cycle. The impact of iron fertilization is also tested in experiments under corresponding glacial conditions. Note that the aim of this study is not to reproduce a transient pCO_2^{atm} drawdown process mimicking the last glacial cycle but to identify key processes accounting for the stepwise pCO_2^{atm} drawdown at different glacial stages.

2. Experimental Design

A state-of-the-art marine biogeochemical model (Regulated Ecosystem Model 2 [REcoM2]; Hauck et al., 2013) coupled to the Massachusetts Institute of Technology ocean general circulation model MITgcm (Campin et al., 2020; Marshall et al., 1997) with a dynamic and thermodynamic sea ice model (Losch et al., 2010), is used to simulate the ocean carbon cycle. Changes of pCO_2^{atm} is calculated with an atmospheric CO_2 box in REcoM2 (more details in Supporting Information S1).

To elaborate on the key processes driving the stepwise glacial pCO_2^{atm} drawdown, we designed a series of snapshot experiments representing idealized interglacial, early-glacial, later- (or full-) glacial conditions, where the "later-glacial" is specified as the LGM-like state. The glacial stages are characterized by changes in different key processes (Figure S1 in Supporting Information S1) and were simulated by using perturbed atmospheric forcings (see Supporting Information S1). Model outputs from a fully-coupled climate model study (Zhang et al., 2013, more details in Supporting Information S1) are used here as forcing fields, that is, the monthly data from the last 100 years (1,200 months) of the 3,000-year Pre-Industrial (PI) run and the 4,000-year LGM run. The following experiments are presented in this paper (Table 1).

First, IG_ctl representing the interglacial conditions, driven by the PI forcing data. We are aware that orbital forcing and thus insolation might differ among different interglacials (e.g., Otto-Bliesner et al., 2021; Tzedakis et al., 2009). However, since the main focus is to assess the role of IG-G SST changes on the carbon cycle, we chose PI to represent general IG conditions for a generic process understanding. In addition, the carbon cycle in IG_ctl is corroborated and validated by observations, providing a basis for following sensitivity experiments (see Supporting Information S1).

Table 1
Experimental Design and Atmospheric Box Output

	Experimental design and atmospheric box output						
	SO		NA	NP			
Exp. name	Dust	Cooling	Cooling	Cooling	pCO_2^{atm} (ppm)	Diff. (ppm)	Use_nice (ppm)
IG_ctl	IG	x	x	x	276	–	−1
IG_Gso	IG	✓	x	x	254	−22	−2
IG_Gna	IG	x	✓	x	282	+6	//
IG_Gp	IG	x	x	✓	278	+2	//
IG_Gns	IG	✓	✓	x	250	−26	+2
IG_Gps	IG	✓	x	✓	253	−23	//
IG_Gnps	IG	✓	✓	✓	244	−32	//
IG_Gd	G	x	x	x	263	−13	//
IG_Gnsd	G	✓	✓	x	235	−41	//
G_ctl	G	✓	✓	✓	223	−53	+6

Note. In Table 1, "SO," "NA," and "NP" refer to the Southern Ocean, the North Atlantic, and the North Pacific, respectively. In the "Dust" column, (interglacial) *IG* means the present-day dust deposition map is used, while *G* means the Last Glacial Maximum (LGM) dust deposition map is used. In the "Cooling" columns, "✓" means the specific region(s) is cooled to the LGM state while "x" means the region(s) remains at the interglacial temperature. In the "diff" column, the pCO_2^{atm} difference between the given experiment and "IG_ctl" is showed. In the "Use_nice" column, the pCO_2^{atm} difference between the experiment with or without the "nice" setup (with "nice" setup means sea ice in the experiment does not prevent air-sea CO_2 exchanges, see Section 2) is shown, indicating the barrier effects of the sea ice in the experiments.

Second, six experiments examining the effects of cooling in a single ocean region (NA, NP, or SO) and a combination of several ocean regions. In these experiments, the PI heat flux in the forcing fields is replaced by LGM fields (see Supporting Information S1) so that the SST in specific ocean regions is lowered to the LGM level. We focus here mostly on the effect of cooling in the SO and NA because the AABW and NADW form in these two regions. For comparability, we also did experiments with cooling in the NP. They started from the interglacial condition (IG_ctl) with a part of the ocean cooled to the LGM state: IG_Gna, IG_Gp and IG_Gso for cooling in three single ocean regions: NA, NP, and SO, respectively; IG_Gns, IG_Gps and IG_Gnps for cooling combined by two (NA and SO or NP and SO) or three regions (NA, NP, and SO), respectively. Primarily, these experiments serve to distinguish the effects of different processes and understand their synergy. They are therefore not designed to reproduce specific glacial stages. Nevertheless, some of them can represent key characteristics of an earlier or later glacial stage, hinting roles of associated key operating processes. For example, proxies showed that during the early glacial time (roughly MIS 5e to 5d), the surface SO experienced a drastic cooling of ∼2.5°C, close to the temperature at the LGM (Figure S1d in Supporting Information S1). During this period, the SO sea ice also expanded (Figure S1e in Supporting Information S1), in agreement with the results of IG_Gso (Figure 2a). Therefore, we consider IG_Gso as an idealized early-glacial condition. We also assumed that IG_Gns to some extent represents a later-glacial physical condition, since the deep-water formation regions in both hemispheres are cooled to the LGM state in this experiment, which could produce an LGM-like deep ocean. This assumption is verified by analysis of the experiment results (Section 3 and 4).

Third, two iron fertilization experiments with the glacial dust deposition over the SO: IG_Gd under otherwise interglacial conditions and IG_Gnsd combined with cooling in the NA and SO. The latter might represent a later glacial-like period when a typical cold and dry glacial state is established (e.g., LGM; Martínez-García et al., 2014; Shaffer & Lambert, 2018) and dust deposition is enhanced.

Fourth, G_ctl represents the full maximal glacial conditions. The forcing fields of this simulation were taken from the LGM (∼21 ka) simulation (the LGMW experiment; Zhang et al., 2013), with an LGM dust deposition map (Albani et al., 2014).

Additionally, four experiments, with a "_nice" setup ("Use_nice" column in Table 1), were carried out to investigate the "barrier effect" of SO sea ice, in which the SO sea ice was ignored in calculating the air-sea CO_2

exchange. Other sea ice-associated processes, such as both physical (e.g., brine rejection) and biological (e.g., light penetration), were kept unchanged.

As these changes (i.e., surface cooling, sea ice expansion, and iron fertilization) differed clearly through the course of glaciation, our experiments enable to pin down key operating processes at different stages of the last glacial cycle, although we cannot reproduce transient features of glacial pCO_2^{atm} drawdown.

3. Results and Discussion

3.1. Distinct Carbon Cycle Responses to the Northern/Southern Hemisphere Surface Cooling

Responses of pCO_2^{atm} to the imposed temperature change are substantially different between the experiments in which the SO and NA were cooled to the maximal glacial state individually or together (Table 1). pCO_2^{atm} in IG_Gso shows a considerable decrease of 22 ppm compared to IG_ctl, whereas a small increase of 6 ppm is obtained in IG_Gna. Combined cooling in the SO and NA (IG_Gns) results in a significantly larger pCO_2^{atm} drawdown than adding up the pCO_2^{atm} changes in IG_Gna and IG_Gso, indicating a nonlinear relationship of carbon sequestration processes in the SO and NA. Cooling in the NP generally results in minor changes in pCO_2^{atm}, unless combined with the SO and NA cooling (IG_Gnps). These distinct pCO_2^{atm} responses to cooling in different regions can be explained based on changes in the ocean circulation (Figure S3 in Supporting Information S1) and marine carbon storage (Figure 1 and Figure S2 in Supporting Information S1). We here focus on four key experiments, namely IG_ctl, IG_Gso, IG_Gns, and G_ctl (Figure 1).

Due to the cooling and the consequential sea ice expansion in the SO (IG_Gso, Figure 1b), colder and saltier (hence denser) water forms at the surface and descends into the ocean interior as AABW. The model uses the KPP vertical mixing scheme by Large et al. (1994), which includes a Richardson-number dependent interior mixing, so changes in stratification affect diapycnal mixing. The increased stratification would hinder the diapycnal mixing between the two overturning cells, weakening the carbon exchange between them and keeping more carbon stored in the deep ocean. Another mechanism contributing to pCO_2^{atm} drawdown is the shortening of surface SO exposure time (the transit time of a water mass in the southern branch of the SO circulation) (Stein et al., 2020). Following the calculation by Stein et al. the exposure time in IG_ctl, IG_Gso, IG_Gns, G_ctl is 315, 76, 58, and 26 days, respectively (see Supporting Information S1 for the calculation). Under glacial (G_ctl) and interglacial conditions (IG_ctl), our results are in line with Stein et al. (2020). With shorter exposure time, carbon-rich upwelled waters cannot undergo complete gas exchange with the atmosphere, leading to higher carbon storage in the ocean. Hence, the carbon storage in the mid- to deep-Atlantic and the SO is enlarged (Figure 1b), leading to lower pCO_2^{atm}. With the expansion of deep Pacific overturning circulation (Figure S3 in Supporting Information S1) in the Pacific Ocean, more carbon leaks from the deep and intermediate waters into the surface ocean, resulting in a negative dissolved inorganic carbon (DIC) anomaly in the deep NP.

In IG_Gna, the surface NA cooling results in a stronger (over 24 Sv) and deeper AMOC (Figure S3b in Supporting Information S1), associated with a reduction of deep stratification (Figures S4b and S5b in Supporting Information S1). The vertical gradient of DIC thus decreases with a strong positive DIC anomaly in the upper overturning cell and a negative anomaly in the lower one (Figure S2b in Supporting Information S1). The positive DIC anomaly in the upper ocean promotes ocean outgassing and increases pCO_2^{atm}, even though the solubility pump in the NA is enhanced due to cooling.

In IG_Gns, when both NA and SO cooling are considered, the combined effects of enhanced solubility pump and downward DIC transport by NADW in the NA with strengthened AABW formation and deep stratification in the SO (Figure 1c) promote more carbon storage in the deep Atlantic and SO than in experiment IG_Gso. Both the salinity and DIC anomaly in IG_Gns represent the later-glacial ocean state in the Atlantic and the SO, whereas the impact of the Pacific is neglected. Further, configured with the LGM boundary conditions, G_ctl represents the full glacial ocean.

Overall, these experiments reveal that the cooling of the SO can result in a marked pCO_2^{atm} drawdown by strengthening deep stratification and shortening the surface exposure time for the air-sea gas exchange. Cooling in the NA mainly affects the solubility pump (Figure S6 in Supporting Information S1) and the deepwater formation (Figures S3–S5 in Supporting Information S1). Whether the carbon taken up by the enhanced solubility pump

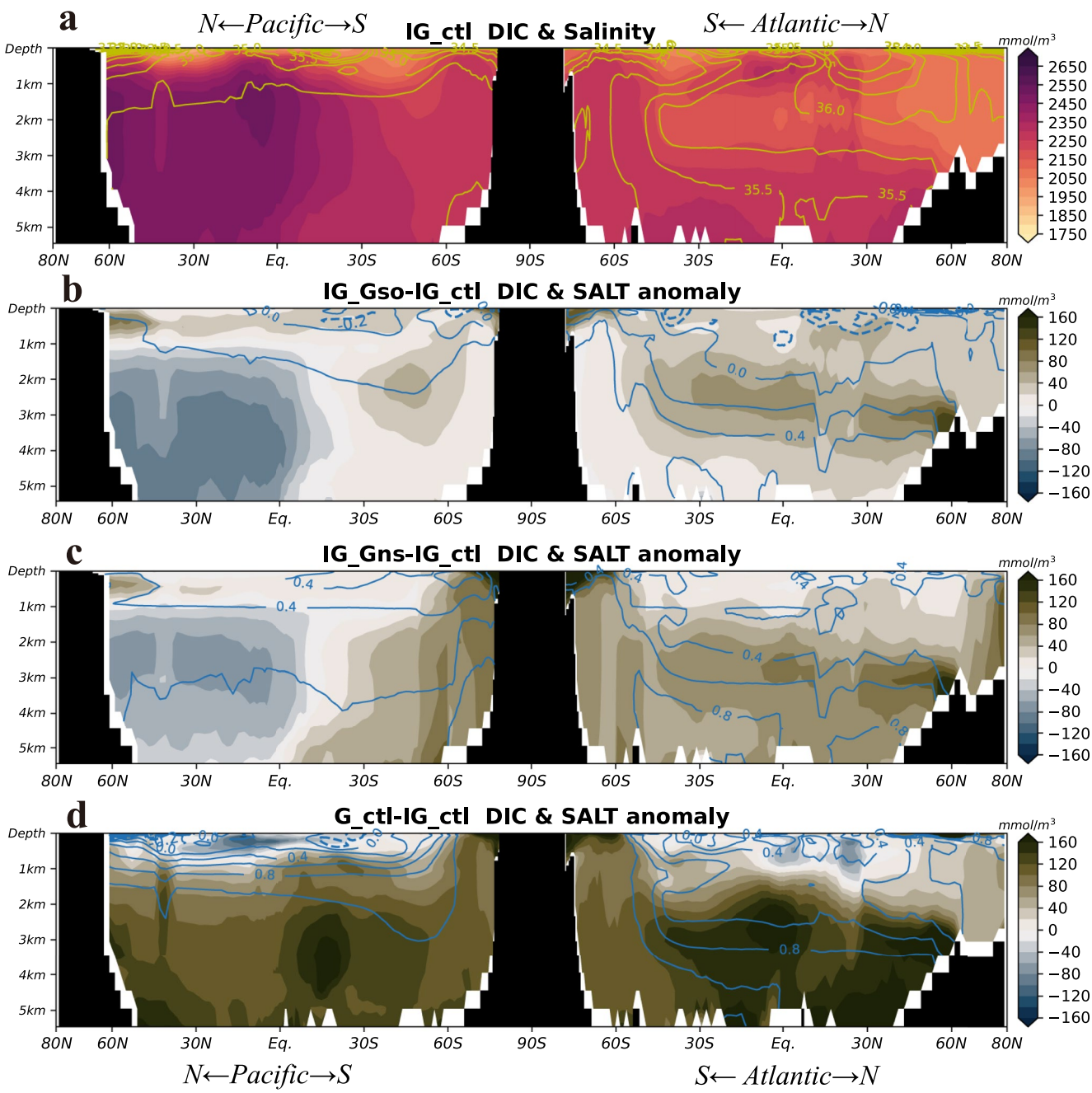

Figure 1. Dissolved inorganic carbon (DIC) concentration (shaded) and salinity (contours, in ‰) transects in key experiments. In each plot, the transect runs from the North Pacific on the left, through the Southern Ocean in the middle, and to the North Atlantic on the right. Note that modeled DIC concentration and salinity in IG_ctl are shown in panel (a) whereas in panels (b–d) the anomalies are shown. In panels (b–d), positive salinity anomalies are shown as solid lines while negative values as dashed lines. Note that from IG_ctl to IG_Gso and then to IG_Gns, the deep ocean salinity in both the Atlantic and Pacific exhibits a clear increase, indicating gradual establishment of the deep stratification in these experiments.

can be stored in the deep ocean or not is, however, controlled by the existence of an enhanced AABW and thus an LGM-like stratified ocean. Cooling in the NP alone results in a negligible change in carbon storage (Table 1). Nevertheless, the NP can facilitate carbon storage when cooling in NA and SO is taken into account. Taken together, the SO processes initialize the long-term carbon uptake in the course of glaciation, after which the processes induced by cooling in NA and NP further promote carbon input into the ocean.

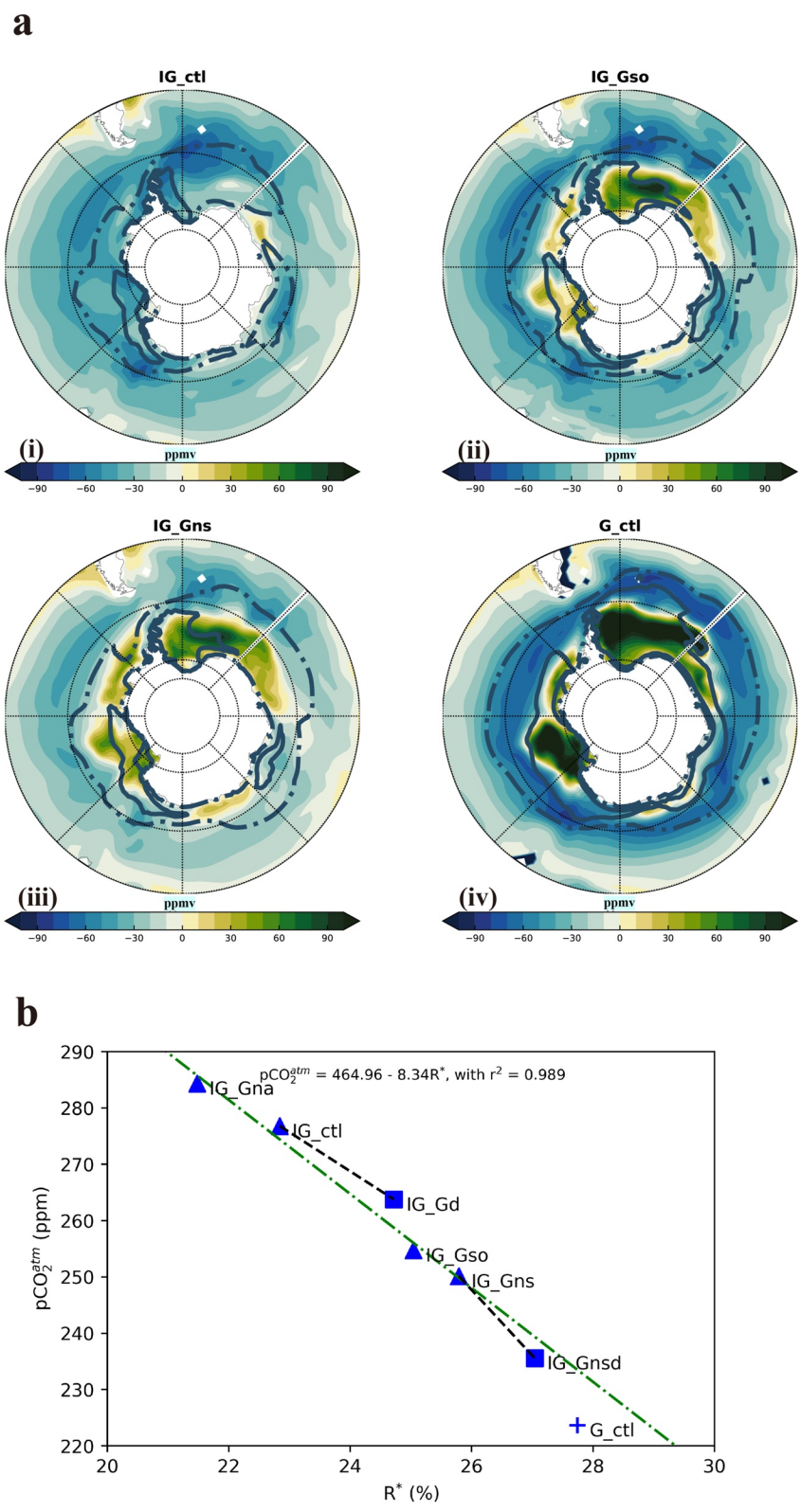
a
IG_ctl
IG_Gso
IG_Gns
G_ctl
(i)
(ii)
(iii)
(iv)
ppmv
−90 −60 −30 0 30 60 90
b
pCO_2^{atm} = 464.96 - 8.34R*, with r^2 = 0.989
IG_Gna
IG_ctl
IG_Gd
IG_Gso
IG_Gns
IG_Gnsd
G_ctl
pCO_2^{atm} (ppm)
R* (%)
290 280 270 260 250 240 230 220
20 22 24 26 28 30

Figure 2.

3.2. Climate-Dependent Roles of the SO Sea Ice Barrier Effects

The SO sea ice has been acknowledged to account for the glacial pCO_2^{atm} drawdown. Comparing the two control runs IG_ctl and G_ctl, the modeled maximal SO sea ice cover grows by ∼100% during LGM (Figures S7a and S7b in Supporting Information S1). On the one hand, the stronger glacial sea ice formation (Gersonde et al., 2005) and subsequent brine rejection effects (Marzocchi & Jansen, 2017) might cause denser bottom water production and thus stronger deep stratification, as supported by the modeled salinity and carbon storage in the deep ocean (Figure 1). On the other hand, sea ice cover can act as a lid on sea surface, hindering the air-sea gas exchange, known as the so-called "barrier effect" (Kohfeld & Chase, 2017). Key regions at the high-latitude SO (e.g., Weddell Sea and Ross Sea) are the main locations of upwelling of the carbon-rich water from both deepwater cells. Thus, an extended sea ice cover could reduce the outgassing in the SO. Kohfeld and Chase (2017) proposed that the barrier effect drove the initial pCO_2^{atm} drawdown at the last glacial inception.

To investigate the impact of the barrier effect, particularly regarding the expanding degree of SO sea ice and ocean circulation pattern under different climate states, we conducted four simulations with the *_nice setup (see Section 2, Table 1), in which sea ice was formed in the same way as in the corresponding simulations without the suffix "_nice", but the sea ice cover does not prevent the air-sea gas exchange. Under the LGM condition (G_ctl_nice vs. G_ctl), the barrier effect lowers pCO_2^{atm} by 6 ppm, ∼10% of the modeled glacial pCO_2^{atm} drawdown, comparable to the fraction estimated in previous studies (Chikamoto et al., 2012; Khatiwala et al., 2019). Under the interglacial condition (IG_ctl_nice vs. IG_ctl), however, the barrier effect leads to a negligible pCO_2^{atm} change of 1 ppm. Similar pCO_2^{atm} changes are simulated in the SO cooling experiments (IG_Gso/IG_Gso_nice), indicating the barrier effect may not contribute to the early-glacial pCO_2^{atm} drawdown. When both the SO and the NA are cooled to the glacial state (IG_Gns vs. IG_Gns_nice) the pCO_2^{atm} drawdown caused by the barrier effect increases to 2 ppm.

The nonlinear impact of sea ice cover on pCO_2^{atm} indicates that not only the extension of sea ice cover plays a role, but the potential net carbon exchange prevented by the ice cover is also important, as can be seen in the sea surface-air pCO_2 difference ($d\,pCO_2$, Figure 2a). In the interglacial state (IG_ctl), when pCO_2^{atm} is high, $d\,pCO_2$ (namely $pCO_2(surface) - pCO_2(atm)$) in the SO is overall negative, that is, without the barrier effect of sea ice, the SO would take up more CO_2. During the full glacial state (G_ctl), however, $d\,pCO_2$ is strongly positive beneath the permanent sea ice cover. This region would undergo intensive CO_2 outgassing without the sea ice barrier, which outweighs the uptake tendency under the seasonal sea ice cover. Thus, how the sea ice cover affects the air-sea gas exchange strongly depends on the relative location of the ice cover and the $d\,pCO_2$ pattern. In IG_Gso and IG_Gns, the expansion of sea ice does not change significantly, whereas a positive $d\,pCO_2$ is found in IG_Gns in a larger area caused by the stronger stratification and lower pCO_2^{atm}. The barrier effect of sea ice cover on ocean outgassing thus increases, when the climate background changes from the interglacial (IG_ctl) across the early glacial stage (IG_Gso) to the full glacial state (G_ctl).

3.3. Iron Fertilization and the Southern Ocean Contribution to the Global Export Production

We quantified the effect of iron fertilization on the marine biological carbon pump under interglacial (IG_Gd) as well as later glacial (IG_Gnsd) climate conditions. Under the interglacial condition (IG_Gd), the dust fertilization over the SO results in a pCO_2^{atm} drawdown of 13 ppm. Together with the cooling of SO and NA (IG_Gnsd), pCO_2^{atm} decreases additionally by 15 ppm compared to IG_Gns. Modeled pCO_2^{atm} drawdown(s) in these experiments (IG_Gd vs. IG_ctl, and IG_Gnsd/IG_Gns) is generally in line with previous modeling work (∼42 to ∼16 ppm) compiled by Gottschalk et al. (2019).

Iron fertilization during LGM does not lead to an increase of export production in our simulations. Both the global and SO EP in G_ctl (4.63/1.28 Gt C $year^{-1}$) are lower than those in IG_ctl (6.05/1.38 Gt C $year^{-1}$). It is

Figure 2. (a) Modeled sea ice cover and sea-air $d\,pCO_2$. Dashed/solid contours mark annual mean sea ice concentration = 0.9/0.15. Shaded area is $d\,pCO_2$ (calculated by $pCO_2(surface) - pCO_2(atm)$). (b) Linear regression of modeled R^* versus pCO_2^{atm},where R^* = EP(SO)/EP(Global) × 100%. EP refers to export production, defined as carbon sinks out of 100 m depth. The green line is the correlation between R^* and pCO_2^{atm}, which can be described with $pCO_2^{atm} = 464.96 - 8.34 \times R^*$, with $r^2 = 0.989$. The black-dashed line between IG_ctl and IG_Gd refers the pCO_2^{atm} drawdown due to change in dust deposition under warmer (interglacial) conditions, while the line between IG_Gns and IG_Gnsd under colder conditions, with a greater slope. Key experiments in this study are shown as blue triangles (IG_ctl and three cooling experiments), squares (two iron fertilization experiments), and a cross (G_ctl). Details of these experiments are given in Table 1 and Section 2.

still debated whether the EP (SO) in glacial periods was higher or lower than in interglacials. Based on paleoceanographic records, the EP in the Antarctic Zone is proposed to be lower while the EP in the Subantarctic Zone is higher (Ai et al., 2020; Jaccard et al., 2013; Kohfeld et al., 2005; Sigman et al., 2010). One model study showed that the glacial EP(SO) is overall higher despite the lower global EP (Yamamoto et al., 2019), while some other models argued that it may behave in an opposite way (Buchanan et al., 2016; Marzocchi & Jansen, 2019) caused by the low temperature and expanded sea ice area.

To explain how iron fertilization over the SO contributes to the pCO_2^{atm} drawdown despite the lower export production, we defined the contribution of the SO export production [EP (SO)] to the global export production [EP (Global)], as $R^* = \mathrm{EP(SO)}/\mathrm{EP(Global)} \times 100\%$ (Table S2 in Supporting Information S1). Iron fertilization increases R^* under both colder (IG_Gnsd and IG_Gns) and warmer (IG_Gd vs. IG_ctl) conditions (dashed black lines in Figure 2b); while the increase of R^* under colder conditions acts more efficiently on pCO_2^{atm} drawdown than under warm conditions (slope of dashed black lines). These results reveal a higher efficiency of the marine biological pump during colder climate stages with high dust deposition: more biologically carbon fixation is shifted to the SO and can be transported into the ocean interior due to changes in ocean circulation and stratification.

4. Synthesis

It is challenging to investigate links between different mechanisms driving the pCO_2^{atm} variability during glacial cycles. We here tentatively disentangle the roles of some key mechanisms in the ocean and their synergy at the different stages of glacial pCO_2^{atm} drawdown. After examining the changes caused by single or combined mechanisms in idealized equilibrium snapshot experiments, we provide here a conceptual diagram to represent key processes accounting for pCO_2^{atm} drawdown at different stages during a glacial cycle (Figure 3).

Under interglacial conditions, supply of the bioavailable iron in the SO is lower than that under glacial conditions, and the NA carbon uptake is rather weak due to the warm SSTs (Figure 3a). At the last glacial inception, pCO_2^{atm} decreases by ~35 ppm (Figure S1a in Supporting Information S1), with a drastic drop of the surface temperature in the SO (Figure S1d in Supporting Information S1), and a clear SO sea ice expansion (Figure S1e in Supporting Information S1), but the dust supply is still at the interglacial level (Martínez-García et al., 2014). It is thus plausible to consider the SO cooling as the key mechanism accounting for pCO_2^{atm} change. The experiment IG_Gso shows that the SO cooling can trigger an initial pCO_2^{atm} drawdown by shortening the surface exposure time (as also proposed by Stein et al. (2020)) and establishing deep stratification (Figure 3b). Nevertheless, the experiment with the same setup but ignoring the blocking effect of sea ice on the air-sea gas exchange (IG_Gso_nice) reveals that sea ice expansion during early-glacial time does not necessarily prevent ocean outgassing. Because pCO_2^{atm} is still sufficiently high, a vast ocean area characterized by the seasonal sea ice tends to take CO_2 from the atmosphere (see the green-white block under the sea ice cover in Figure 3b). On the other hand, in IG_Gna the drastic cooling (~8°C, much more than the ~3°C cooling of the SO) does not lead to more ocean carbon storage, supporting that the cooling in the SO is the key driver of pCO_2^{atm} drawdown at the early-glacial time.

Associated with the cooling of the SO, the NA is also cooled to the glacial state in IG_Gns. Compared to IG_ctl, the colder and saltier AABW occupies a much larger volume in the ocean interior, increasing the deep carbon storage (Figure S3 in Supporting Information S1). Meanwhile, the NA uptake is more enhanced by the meridional SST gradients (Yu et al., 2019) compared to the interglacial state (Figure S6 in Supporting Information S1). It is noteworthy that the comparison of IG_Gns and IG_Gna (cooling in the NA) shows that the enhanced NA carbon sequestration is largely dependent on the deep ocean stratification established by the SO cooling, as cooling the NA alone even slightly increases pCO_2^{atm}. This clearly demonstrates an interhemispheric synergy of processes in carbon sequestration and emphasizes the fundamental role of SO in providing a basis to store more carbon in the deep ocean. Later in the glacial cycle, pCO_2^{atm} becomes low (Figure S1a in Supporting Information S1, Table 1), the SO tends to release carbon to the atmosphere (Figure 2a); hence the expanded sea ice cover suppresses local carbon leakage, as found in G_ctl_nice and in previous studies (Morales Maqueda & Rahmstorf, 2002; Stephens & Keeling, 2000). Additionally, throughout a glacial cycle, the NP appears to be a passive carbon reservoir responding to changes in the deep Pacific overturning circulation (Figures S2 and S3 in Supporting Information S1).

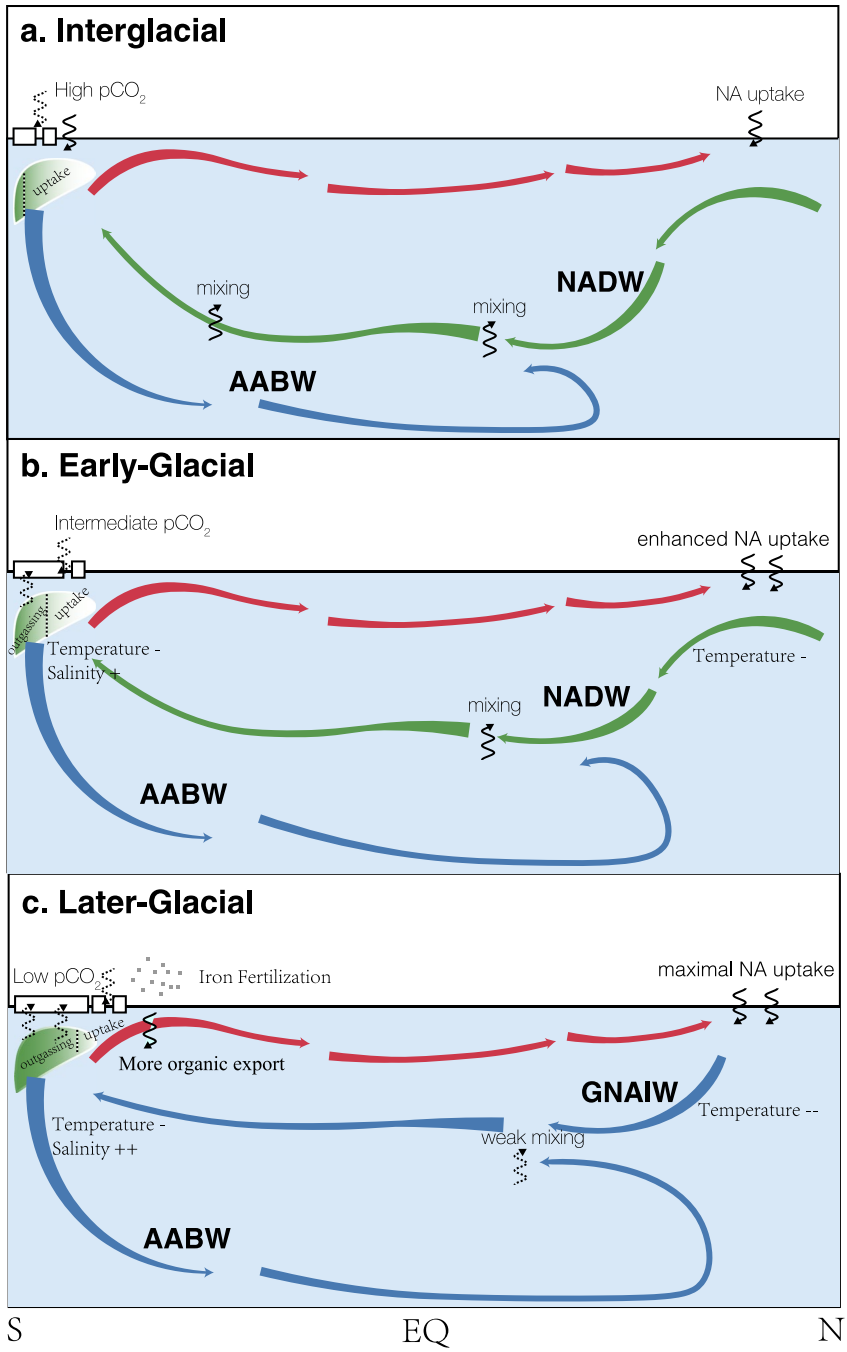

Figure 3. Conceptual diagram for temporal evolution of the glacial pCO_2 drawdown. The three subplots are the idealized scenarios (demonstrated in the Atlantic Basin) in interglacial (a), early-glacial (b), and later-glacial (c) state, respectively. Solid curved arrows roughly depict the thermohaline circulation indicated by model studies and paleoceanographic proxies (see main text). NADW = North Atlantic Deep Water. GNAIW = Glacial North Atlantic Intermediate Water. AABW = Antarctic Bottom Water. The white boxes in different sizes over the surface ocean in the south represent the Southern Ocean (SO) sea ice cover. The green-white shading under the SO sea ice roughly marks the gradual increase of DIC concentration southward. The black-dashed line in the shading area roughly marks the boundary of the area under sea ice between net outgassing and net uptake. During glaciation (from panels (a) to (c)), the deep ocean becomes colder and saltier, associated with the gradual shoaling of the Atlantic meridional overturning circulation (i.e., NADW to GNAIW) and stronger stratification, weakening the mixing between bottom and intermediate water masses. North Atlantic cooling is strengthened and the solubility pump is enhanced. At the later-glacial stage (c), enhanced dust deposition considerably fertilizes the SO and increases the biological carbon pump. The additional carbon can be stored in the more stratified deep ocean, reducing CO_2 in the atmosphere. As the atmospheric pCO_2 is decreasing and the oceanic DIC increasing, together with the rising sea ice extension during glaciation, the "barrier effect" of sea ice shifts from preventing oceanic uptake of CO_2 to blocking oceanic outgassing.

Furthermore, increased dust deposition at the fully developed glacial state (G_ctl) raises the contribution of the SO in the global biological pump (larger R^*), indicating a higher efficiency of deep sequestration of regenerated carbon, as also found in previous studies (e.g., Kumar et al., 1995). In Figure 2b, we further found a clear negative relationship between R^* and pCO_2^{atm} in IG_ctl together with three cooling experiments that can be fitted to:

$$pCO_2^{atm} = 464.96 - 8.34 \times R^*$$

with $r^2 = 0.989$ (Figure 2b). The regression line (green) can roughly represent the gradual cooling of the oceans (IG_ctl, IG_Gso, IG_Gns, and to G_ctl). Figure 2b shows that the SO contribution to the global marine biological pump is increasing from the early- to later-glacial stages. This is mainly caused by impacts of changing ocean circulation on nutrient distribution (Kwon et al., 2012), as well as by response of phytoplankton under variable growth conditions (e.g., Bradtmiller et al., 2006; Matsumoto & Sarmiento, 2008). Iron fertilization in later-glacial stages further strengthens the contribution of the SO biological pump (IG_Gns to IG_Gnsd).

Based on equilibrium sensitivity experiments, we elaborate the contributions of processes responsible for glacial pCO_2^{atm} drawdown at idealized stages of a glaciation. Given the potential nonlinear feedback among them, transient experiments applying the changing boundary conditions of the last glacial cycle are highly desirable to assess the proposed bipolar synergy on glacial pCO_2^{atm} drawdown.

Conflict of Interest

The authors declare no conflicts of interest relevant to this study.

Data Availability Statement

All model output in this study has been deposited on PANGAEA (https://doi.org/10.1594/PANGAEA.935084). Code of MITgcm can be acquired at https://mitgcm.org/source-code/.

Acknowledgments
J. Du and J. Tian are funded by the NSFC (Grant Nos. 42030403, 42188102, and 41525020) and the State Key Laboratory of Marine Geology, Tongji University (MG202104). J. Tian receives support from the 4th National High-level personnel of special support program of China. X. Zhang is funded by the NSFC (Grant No. 42075047). Y. Ye and C. Völker are funded by the German BMBF project PalMod (Grant No. 01LP1919A). Dr. Jimin Yu is thanked for his constructive discussion about the manuscript. Ms. Sanshan Wei is thanked for her help and guidance about the color schemes of figures. The computational resources were provided by the AWI supercomputer "Ollie". J. Du thanks the China Scholarship Council for providing financial support during his stay in Germany. The authors would like to thank the editor and five anonymous reviewers for the constructive comments on the manuscript.

References

Adkins, J. F. (2002). The salinity, temperature, and $\delta^{18}O$ of the glacial deep ocean. *Science*, *298*(5599), 1769–1773. https://doi.org/10.1126/science.1076252

Ai, X. E., Studer, A. S., Sigman, D. M., Martínez-García, A., Fripiat, F., Thöle, L. M., et al. (2020). Southern Ocean upwelling, Earth's obliquity, and glacial-interglacial atmospheric CO_2 change. *Science*, *370*(6522), 1348–1352. https://doi.org/10.1126/science.abd2115

Albani, S., Mahowald, N. M., Perry, A. T., Scanza, R. A., Zender, C. S., Heavens, N. G., et al. (2014). Improved dust representation in the Community Atmosphere Model. *Journal of Advances in Modeling Earth Systems*, *6*(3), 541–570. https://doi.org/10.1002/2013MS000279

Bradtmiller, L. I., Anderson, R. F., Fleisher, M. Q., & Burckle, L. H. (2006). Diatom productivity in the equatorial Pacific Ocean from the last glacial period to the present: A test of the silicic acid leakage hypothesis. *Paleoceanography*, *21*(4), 1–12. https://doi.org/10.1029/2006PA001282

Buchanan, P. J., Matear, R. J., Lenton, A., Phipps, S. J., Chase, Z., & Etheridge, D. M. (2016). The simulated climate of the Last Glacial Maximum and insights into the global marine carbon cycle. *Climate of the Past*, *12*(12), 2271–2295. https://doi.org/10.5194/cp-12-2271-2016

Campin, J.-M., Heimbach, P., Losch, M., Forget, G., Hill, E., Adcroft, A., et al. (2020). MITgcm/MITgcm: Mid 2020 version. https://doi.org/10.5281/ZENODO.3967889

Chikamoto, M. O., Abe-Ouchi, A., Oka, A., Ohgaito, R., & Timmermann, A. (2012). Quantifying the ocean's role in glacial CO_2 reductions. *Climate of the Past*, *8*(2), 545–563. https://doi.org/10.5194/cp-8-545-2012

Curry, W. B., & Oppo, D. W. (2005). Glacial water mass geometry and the distribution of $\delta^{13}C$ of ΣCO_2 in the western Atlantic Ocean. *Paleoceanography*, *20*(1), PA1017. https://doi.org/10.1029/2004PA001021

Ferrari, R., Jansen, M. F., Adkins, J. F., Burke, A., Stewart, A. L., & Thompson, A. F. (2014). Antarctic sea ice control on ocean circulation in present and glacial climates. *Proceedings of the National Academy of Sciences of the United States of America*, *111*(24), 8753–8758. https://doi.org/10.1073/pnas.1323922111

Gersonde, R., Crosta, X., Abelmann, A., & Armand, L. (2005). Sea-surface temperature and sea ice distribution of the Southern Ocean at the EPILOG Last Glacial Maximum—A circum-Antarctic view based on siliceous microfossil records. *Quaternary Science Reviews*, *24*(7–9), 869–896. https://doi.org/10.1016/j.quascirev.2004.07.015

Gottschalk, J., Battaglia, G., Fischer, H., Frölicher, T. L., Jaccard, S. L., Jeltsch-Thömmes, A., et al. (2019). Mechanisms of millennial-scale atmospheric CO_2 change in numerical model simulations. *Quaternary Science Reviews*, *220*, 30–74. https://doi.org/10.1016/j.quascirev.2019.05.013

Hain, M. P., Sigman, D. M., & Haug, G. H. (2010). Carbon dioxide effects of Antarctic stratification, North Atlantic Intermediate Water formation, and subantarctic nutrient drawdown during the last ice age: Diagnosis and synthesis in a geochemical box model. *Global Biogeochemical Cycles*, *24*(4), 1–19. https://doi.org/10.1029/2010GB003790

Hauck, J., Völker, C., Wang, T., Hoppema, M., Losch, M., & Wolf-Gladrow, D. A. (2013). Seasonally different carbon flux changes in the Southern Ocean in response to the southern annular mode. *Global Biogeochemical Cycles*, *27*(4), 1236–1245. https://doi.org/10.1002/2013GB004600

Hülse, D., Arndt, S., Wilson, J. D., Munhoven, G., & Ridgwell, A. (2017). Understanding the causes and consequences of past marine carbon cycling variability through models. *Earth-Science Reviews*, *171*(September 2016), 349–382. https://doi.org/10.1016/j.earscirev.2017.06.004

Jaccard, S. L., Hayes, C. T., Martínez-García, A., Hodell, D. A., Anderson, R. F., Sigman, D. M., & Haug, G. H. (2013). Two modes of change in Southern Ocean productivity over the past million years. *Science*, *339*(6126), 1419–1423. https://doi.org/10.1126/science.1227545

Jacobel, A. W., Anderson, R. F., Winckler, G., Costa, K. M., Gottschalk, J., Middleton, J. L., et al. (2019). No evidence for equatorial Pacific dust fertilization. *Nature Geoscience*, *12*(3), 154–155. https://doi.org/10.1038/s41561-019-0304-z

Khatiwala, S., Schmittner, A., & Muglia, J. (2019). Air-sea disequilibrium enhances ocean carbon storage during glacial periods. *Science Advances*, *5*(6), eaaw4981. https://doi.org/10.1126/sciadv.aaw4981

Kohfeld, K. E., & Chase, Z. (2017). Temporal evolution of mechanisms controlling ocean carbon uptake during the last glacial cycle. *Earth and Planetary Science Letters*, *472*, 206–215. https://doi.org/10.1016/j.epsl.2017.05.015

Kohfeld, K. E., Le Quéré, C., Harrison, S. P., & Anderson, R. F. (2005). Role of marine biology in glacial-interglacial CO_2 cycles. *Science*, *308*(5718), 74–78. https://doi.org/10.1126/science.1105375

Kumar, N., Anderson, R. F., Mortlock, R. A., Froelich, P. N., Kubik, P., Dittrich-Hannen, B., & Suter, M. (1995). Increased biological productivity and export production in the glacial Southern Ocean. *Nature*, *378*(6558), 675–680. https://doi.org/10.1038/378675a0

Kurahashi-Nakamura, T., Abe-Ouchi, A., & Yamanaka, Y. (2010). Effects of physical changes in the ocean on the atmospheric pCO_2: Glacial-interglacial cycles. *Climate Dynamics*, *35*(4), 713–719. https://doi.org/10.1007/s00382-009-0609-5

Kwon, E. Y., Hain, M. P., Sigman, D. M., Galbraith, E. D., Sarmiento, J. L., & Toggweiler, J. R. (2012). North Atlantic ventilation of southern-sourced deep water in the glacial ocean. *Paleoceanography*, *27*(2), 1–12. https://doi.org/10.1029/2011PA002211

Large, W. G., McWilliams, J. C., & Doney, S. C. (1994). Oceanic vertical mixing: A review and a model with a nonlocal boundary layer parameterization. *Reviews of Geophysics*, *32*(4), 363. https://doi.org/10.1029/94RG01872

Lippold, J., Luo, Y., Francois, R., Allen, S. E., Gherardi, J., Pichat, S., et al. (2012). Strength and geometry of the glacial Atlantic Meridional Overturning Circulation. *Nature Geoscience*, *5*(11), 813–816. https://doi.org/10.1038/ngeo1608

Losch, M., Menemenlis, D., Campin, J.-M., Heimbach, P., & Hill, C. (2010). On the formulation of sea-ice models. Part 1: Effects of different solver implementations and parameterizations. *Ocean Modelling*, *33*(1–2), 129–144. https://doi.org/10.1016/j.ocemod.2009.12.008

Lüthi, D., Le Floch, M., Bereiter, B., Blunier, T., Barnola, J.-M., Siegenthaler, U., et al. (2008). High-resolution carbon dioxide concentration record 650,000–800,000 years before present. *Nature*, *453*(7193), 379–382. https://doi.org/10.1038/nature06949

Marshall, J., Hill, C., Perelman, L., & Adcroft, A. (1997). Hydrostatic, quasi-hydrostatic, and nonhydrostatic ocean modeling. *Journal of Geophysical Research*, *102*(C3), 5733–5752. https://doi.org/10.1029/96JC02776

Marshall, J., & Speer, K. (2012). Closure of the meridional overturning circulation through Southern Ocean upwelling. *Nature Geoscience*, *5*(3), 171–180. https://doi.org/10.1038/ngeo1391

Martin, J. H. (1990). Glacial-interglacial CO_2 change: The iron hypothesis. *Paleoceanography*, *5*(1), 1–13. https://doi.org/10.1029/PA005i001p00001

Martínez-García, A., Sigman, D. M., Ren, H., Anderson, R. F., Straub, M., Hodell, D. A., et al. (2014). Iron fertilization of the Subantarctic Ocean during the last ice age. *Science*, *343*(6177), 1347–1350. https://doi.org/10.1126/science.1246848

Marzocchi, A., & Jansen, M. F. (2017). Connecting Antarctic sea ice to deep-ocean circulation in modern and glacial climate simulations. *Geophysical Research Letters*, *44*(12), 6286–6295. https://doi.org/10.1002/2017GL073936

Marzocchi, A., & Jansen, M. F. (2019). Global cooling linked to increased glacial carbon storage via changes in Antarctic sea ice. *Nature Geoscience*, *12*(12), 1001–1005. https://doi.org/10.1038/s41561-019-0466-8

Matsumoto, K., & Sarmiento, J. L. (2008). A corollary to the silicic acid leakage hypothesis. *Paleoceanography*, *23*(2), 1–9. https://doi.org/10.1029/2007PA001515

Morales Maqueda, M. A., & Rahmstorf, S. (2002). Did Antarctic sea-ice expansion cause glacial CO_2 decline? *Geophysical Research Letters*, *29*(1), 1011. https://doi.org/10.1029/2001GL013240

Oliver, K. I. C., Hoogakker, B. A. A., Crowhurst, S., Henderson, G. M., Rickaby, R. E. M., Edwards, N. R., & Elderfield, H. (2010). A synthesis of marine sediment core $\delta^{13}C$ data over the last 150000 years. *Climate of the Past*, *6*(5), 645–673. https://doi.org/10.5194/cp-6-645-2010

Otto-Bliesner, B. L., Brady, E. C., Zhao, A., Brierley, C. M., Axford, Y., Capron, E., et al. (2021). Large-scale features of Last interglacial climate: Results from evaluating the *lig127k* simulations for the Coupled Model Intercomparison Project (CMIP6)-Paleoclimate Modeling Intercomparison Project (PMIP4). *Climate of the Past*, *17*(1), 63–94. https://doi.org/10.5194/cp-17-63-2021

Rae, J. W. B., & Broecker, W. (2018). What fraction of the Pacific and Indian oceans' deep water is formed in the Southern Ocean? *Biogeosciences*, *15*(12), 3779–3794. https://doi.org/10.5194/bg-15-3779-2018

Shaffer, G., & Lambert, F. (2018). In and out of glacial extremes by way of dust–climate feedbacks. *Proceedings of the National Academy of Sciences of the United States of America*, *115*(9), 2026–2031. https://doi.org/10.1073/pnas.1708174115

Sigman, D. M., & Boyle, E. A. (2000). Glacial/interglacial changes in atmospheric carbon dioxide. *Nature*, *407*(October), 859–869. https://doi.org/10.1038/35038000

Sigman, D. M., Fripiat, F., Studer, A. S., Kemeny, P. C., Martínez-García, A., Hain, M. P., et al. (2020). The Southern Ocean during the ice ages: A review of the Antarctic surface isolation hypothesis, with comparison to the North Pacific. *Quaternary Science Reviews*, *254*, 106732. https://doi.org/10.1016/j.quascirev.2020.106732

Sigman, D. M., Hain, M. P., & Haug, G. H. (2010). The polar ocean and glacial cycles in atmospheric CO_2 concentration. *Nature*, *466*(7302), 47–55. https://doi.org/10.1038/nature09149

Stein, K., Timmermann, A., Kwon, E. Y., & Friedrich, T. (2020). Timing and magnitude of Southern Ocean sea ice/carbon cycle feedbacks. *Proceedings of the National Academy of Sciences of the United States of America*, *117*(9), 4498–4504. https://doi.org/10.1073/pnas.1908670117

Stephens, B. B., & Keeling, R. F. (2000). The influence of Antarctic sea ice on glacial-interglacial CO_2 variations. *Nature*, *404*(6774), 171–174. https://doi.org/10.1038/35004556

Talley, L. D. (2013). Closure of the global overturning circulation through the Indian, Pacific, and Southern Oceans. *Oceanography*, *26*(1), 80–97. https://doi.org/10.5670/oceanog.2013.07

Tzedakis, P. C., Raynaud, D., McManus, J. F., Berger, A., Brovkin, V., & Kiefer, T. (2009). Interglacial diversity. *Nature Geoscience*, *2*(11), 751–755. https://doi.org/10.1038/ngeo660

Wolff, E. W., Fischer, H., Fundel, F., Ruth, U., Twarloh, B., Littot, G. C., et al. (2006). Southern Ocean sea-ice extent, productivity and iron flux over the past eight glacial cycles. *Nature*, *440*(7083), 491–496. https://doi.org/10.1038/nature04614

Yamamoto, A., Abe-Ouchi, A., Ohgaito, R., Ito, A., & Oka, A. (2019). Glacial CO_2 decrease and deep-water deoxygenation by iron fertilization from glaciogenic dust. *Climate of the Past*, *15*(3), 981–996. https://doi.org/10.5194/cp-15-981-2019

Yu, J., Menviel, L., Jin, Z. D., Thornalley, D. J. R., Foster, G. L., Rohling, E. J., et al. (2019). More efficient North Atlantic carbon pump during the Last Glacial Maximum. *Nature Communications*, *10*(1), 1–11. https://doi.org/10.1038/s41467-019-10028-z

Zhang, X., Lohmann, G., Knorr, G., & Xu, X. (2013). Different ocean states and transient characteristics in last glacial maximum simulations and implications for deglaciation. *Climate of the Past*, *9*(5), 2319–2333. https://doi.org/10.5194/cp-9-2319-2013

References From the Supporting Information

Antonov, J. I., Seidov, D., Boyer, T. P., Locarnini, R. A., Mishonov, A. V., Garcia, H. E., et al. (2010). World Ocean Atlas 2009, volume 2: Salinity. *World Ocean Atlas 2009*, *2*, 184.

Aumont, O., Ethé, C., Tagliabue, A., Bopp, L., & Gehlen, M. (2015). PISCES-v2: An ocean biogeochemical model for carbon and ecosystem studies. *Geoscientific Model Development*, *8*(8), 2465–2513. https://doi.org/10.5194/gmd-8-2465-2015

Bereiter, B., Eggleston, S., Schmitt, J., Nehrbass-Ahles, C., Stocker, T. F., Fischer, H., et al. (2015). Revision of the EPICA Dome C CO_2 record from 800 to 600 kyr before present. *Geophysical Research Letters*, *42*(2), 542–549. https://doi.org/10.1002/2014GL061957

Brovkin, V., Raddatz, T., Reick, C. H., Claussen, M., & Gayler, V. (2009). Global biogeophysical interactions between forest and climate. *Geophysical Research Letters*, *36*(7), 1–5. https://doi.org/10.1029/2009GL037543

Campin, J.-M., Adcroft, A., Hill, C., & Marshall, J. (2004). Conservation of properties in a free-surface model. *Ocean Modelling*, *6*(3–4), 221–244. https://doi.org/10.1016/S1463-5003(03)00009-X

Garcia, H. E., Locarnini, R. A., Boyer, T. P., Antonov, J. I., Zweng, M. M., Baranova, O. K., & Johnson, D. R. (2010). World Ocean Atlas 2009, volume 4: Nutrients (phosphate, nitrate, silicate). *World Ocean Atlas 2009*, *4*.

Hauck, J., & Völker, C. (2015). Rising atmospheric CO_2 leads to large impact of biology on Southern Ocean CO_2 uptake via changes of the Revelle factor. *Geophysical Research Letters*, *42*(5), 1459–1464. https://doi.org/10.1002/2015GL063070

Lambert, F., Delmonte, B., Petit, J. R., Bigler, M., Kaufmann, P. R., Hutterli, M. A., et al. (2008). Dust-climate couplings over the past 800,000 years from the EPICA Dome C ice core. *Nature*, *452*(7187), 616–619. https://doi.org/10.1038/nature06763

Locarnini, R. A., Mishonov, A. V., Antonov, J. I., Boyer, T. P., Garcia, H. E., Baranova, O. K., et al. (2010). World Ocean Atlas 2009, volume 1: Temperature. *World Ocean Atlas 2009*, *1*(Temperature), 184.

Marsland, S. J., Haak, H., Jungclaus, J. H., Latif, M., & Röske, F. (2002). The Max-Planck-Institute global ocean/sea ice model with orthogonal curvilinear coordinates. *Ocean Modelling*, *5*(2), 91–127. https://doi.org/10.1016/S1463-5003(02)00015-X

Olsen, A., Key, R. M., van Heuven, S., Lauvset, S. K., Velo, A., Lin, X., et al. (2016). The Global Ocean Data Analysis Project version 2 (GLODAPv2) – An internally consistent data product for the world ocean. *Earth System Science Data*, *8*(2), 297–323. https://doi.org/10.5194/essd-8-297-2016

Pagnone, A., Völker, C., & Ye, Y. (2019). Processes affecting dissolved iron across the Subtropical North Atlantic: A model study. *Ocean Dynamics*, *69*(9), 989–1007. https://doi.org/10.1007/s10236-019-01288-w

Roeckner, E., Bäuml, G., Bonaventura, L., Brokopf, R., Esch, M., Giorgetta, M., et al. (2003). *The atmospheric general circulation model ECHAM 5. PART I: Model description* (Report).Max-Planck-Institut Für Meteorologie.

Wei, W., & Lohmann, G. (2012). Simulated Atlantic multidecadal oscillation during the Holocene. *Journal of Climate*, *25*(20), 6989–7002. https://doi.org/10.1175/JCLI-D-11-00667.1

Ye, Y., & Völker, C. (2017). On the role of dust-deposited lithogenic particles for iron cycling in the tropical and subtropical Atlantic. *Global Biogeochemical Cycles*, *31*(10), 1543–1558. https://doi.org/10.1002/2017GB005663

Yu, J., Menviel, L., Jin, Z. D., Anderson, R. F., Jian, Z., Piotrowski, A. M., et al. (2020). Last glacial atmospheric CO_2 decline due to widespread Pacific deep-water expansion. *Nature Geoscience*, *13*(9), 628–633. https://doi.org/10.1038/s41561-020-0610-5

Zhang, X., Barker, S., Knorr, G., Lohmann, G., Drysdale, R., Sun, Y., et al. (2021). Direct astronomical influence on abrupt climate variability. *Nature Geoscience*, *14*(11), 819–826. https://doi.org/10.1038/s41561-021-00846-6

Zhang, X., Knorr, G., Lohmann, G., & Barker, S. (2017). Abrupt North Atlantic circulation changes in response to gradual CO_2 forcing in a glacial climate state. *Nature Geoscience*, *10*(7), 518–523. https://doi.org/10.1038/ngeo2974

Zhang, X., Lohmann, G., Knorr, G., & Purcell, C. (2014). Abrupt glacial climate shifts controlled by ice sheet changes. *Nature*, *512*(7514), 290–294. https://doi.org/10.1038/nature13592